

A Demonstrator for Bolometric Interferometry

Adnan GHRIBI*, Andrea Tartari*†, Silvia Galli*, Michel Piat*, Eric Breelle*, Jean-Christophe Hamilton*,
Sebastiano Spinelli†, Massimo Gervasi†, Mario Zannoni†.

November 1, 2018

Abstract

Bolometric Interferometry (BI) is one of the most promising techniques for precise measurements of the Cosmic Microwave Background polarization. In this paper, we present the results of DIBO (Démonstrateur d'Interférométrie Bolométrique), a single-baseline demonstrator operating at 90 GHz, built to proof the validity of the BI concept applied to a millimeter-wave interferometer. This instrument has been characterized in the laboratory with a detector at room temperature and with a 4 K bolometer. This allowed us to measure interference patterns in a clean way, both (1) rotating the source and (2) varying with time the phase shift among the two interferometer's arms. Detailed modelisation has also been performed and validated with measurements.

Introduction

Scientific Background

The Cosmic Microwave Background (CMB) is a 3K black body radiation last scattered about 300000 years after the Big Bang. Dedicated instruments have observed CMB anisotropies both in temperature (of the order of 10^{-5}) and in polarization. These fluctuations contain precious cosmological information concerning the contents and the dynamics of our Universe. Nevertheless, most of the polarized information remains to be discovered. This is especially the case for the so called B-modes of CMB polarization that are expected to be at least 3 orders of magnitude lower than temperature anisotropies [1]. B-modes could contain the finger print of the hypothetical primordial gravitational waves predicted by Einstein's General Relativity. This is a major challenge in cosmology in which several research groups are involved.

Instrumentation for cosmology & Bolometric Interferometry

Bolometers, cooled to very low temperatures ($<0.3\text{K}$) are the most sensitive detectors for large bandwidth detection in the sub-millimeter and millimeter wavelength range. Their principle of operation is to convert the power carried by the electromagnetic waves into heat through an absorber and to measure its temperature. The measured signal is directly proportional to the incoming power.

*AstroParticule & Cosmologie, Université Paris Diderot

†Radio Group, Università degli Studi di Milano - Bicocca

Many experiences dedicated to CMB measurement are based on bolometric detection (Cobe-FIRAS, Boomerang, Maxima, Archeops, Planck HFI, among others¹). The future ESA Planck mission [3] will use spiderweb bolometers which will operate near the photon noise limit. However, the detection of the B modes requires an improvement of up to two orders of magnitude in sensitivity with respect to the Planck mission. The only solution is therefore to increase the number of detectors.

The CMB polarization characterization is nevertheless not only a question of sensitivity. It also needs an exquisite control of all the instrumental and systematic effects. As an example, for an imager, any lenses or mirrors used to define the beam in the sky are sources of spurious polarization effects that can mask the tiny B-mode signal.

Using an interferometer is an interesting alternative to imager [4]. It directly measures the Fourier transform of the intensity and polarization distribution on the sky. Since only correlated signals are detected, such system is intrinsically less sensitive to parasitic effects. Many groups choosed this direction for the measurement of the CMB polarization. Some interferometers used for that purpose are DASI, CBI and VSA [5]. These experiments use coherent detection techniques where the signal received is amplified before being detected. The amplification is intrinsically noisy leading to less sensitive instruments. Moreover, the correlation need a narrow bandwidth that further reduce the sensitivity.

In order to reach the bolometric sensitivity together with the systematic cleanness of interferometers, we are developing an instrumental concept based on bolometric interferometry : we use adding interferometry combined with bolometric detection. This instrumental concept will be applied to a project called BRAIN/MBI (B Mode Radiation Interferometer / Millimeter-wave Bolometric Interferometer) [6]. This project is an international collaboration targeting the detection and characterization of the B modes with a ground based experiment in the Concordia base (Antarctica). The final instrument will work on three frequency bands (90 GHz, 150 GHz, 220 GHz) with 30% bandwidth for each band. This is needed to subtract the foregrounds and recover a maximum power from the spectrum. The full instrument will be made of 9 modules, each module being made of 12×12 horns. A set of phase shifters in a well defined architecture will allow us to retrieve all the correlations between the different baselines. A first step in the development of such instrument is the proof of concept. For that reason, a simplified instrument DIBO (Démonstrateur d'interférométrie bolométrique) was built with commercial quasi-optical components.

In the first section of this paper, we begin by introducing the instrument and its working principle. We then show its properties and some useful tools for the analysis of the results. The third section describes the different experimental setups developed for DIBO. In the fourth section, the results are shown both for bolometric and power-meter measurements. We finally conclude on perspectives for a next generation bolometric interferometer.

¹see for example [2] for a comprehensive list of experiments

1 The instrument

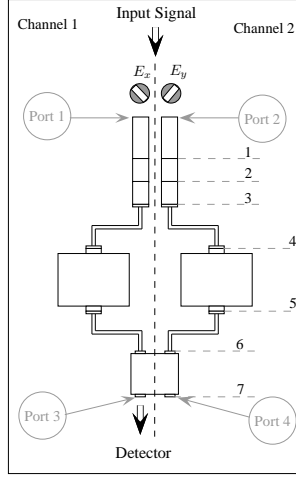


Figure 1: General layout of the instrument design : (1) two corrugated horns, (2) two circular to rectangular transitions, (3) two $\pm 45^\circ$ twists, (4 and 6) four bends, (5) two controllable phase shifters, (7) 90° hybrid coupler.

1.1 Instrument description

The DIBO instrument, as described in figure 1, has two horns pointing toward the same direction. Afterwards, the incoming electromagnetic wave pass through a circular to rectangular (WR10) waveguide transition. The output of this transition allows the selection of a single polarization direction. The two E-planes outputs are orthogonal. After a $\pm 45^\circ$ twist, the waves are phase shifted with controllable phase shifters before being combined by means of a 90° hybrid coupler. The signal is then detected in one at the outputs of the coupler.

1.2 Working principle

The horns are assumed to have the same beam $B(\vec{s})$. They receive the same signals, except that one is out of phase by $\phi_{path} = 2\pi\vec{D}\cdot\vec{s}/\lambda$ compared to the other, where \vec{D} is the separation between the two horns (the baseline), \vec{s} the unitary direction of the incoming radiation and λ the wavelength. This phase shift is purely geometrical and is due to the different optical path to reach each horn antennas. At the output of the antennas, a circular to rectangular transition selects only one linear polarization. By rotating the horns perpendicularly one with respect to the other, we select two perpendicular linear polarizations E_{0x} and E_{0y} on the sky . If we denote with E_x and E_y the two orthogonal components at the outputs of the horns, we can express them by [7]:

$$E_x = \int d^2\vec{s} E_{0x}(\vec{s}) B(\vec{s}) e^{i\omega t} \quad (1)$$

and

$$E_y = \int d^2 \vec{s} E_{0y}(\vec{s}) B(\vec{s}) e^{i[\omega t + \phi_{path}(\vec{s})]}. \quad (2)$$

After that, E_x and E_y are twisted to the same direction in order to be combined. Before being combined, a phase shift $\Delta\alpha$ is introduced with a controllable phase shifter. To simplify, we will consider that the phase shift is introduced in only one of the channels :

$$E'_x = \int d^2 \vec{s} E_{0x}(\vec{s}) B(\vec{s}) e^{i\omega t} \quad (3)$$

$$E'_y = \int d^2 \vec{s} E_{0y}(\vec{s}) B(\vec{s}) e^{i(\omega t + \phi_{path}(\vec{s}) + \Delta\alpha)} \quad (4)$$

Finally, the electromagnetic waves are combined in the 90° hybrid coupler and the power received on each of the outputs over the considered bandwidth is

$$P = \frac{1}{2Z_w} \int EE^* d\nu \quad (5)$$

where Z_w is the wave impedance and E the field resulting from the combination of E'_x and E'_y . After calculation, the detected power is given by the following expression:

$$\langle |E|^2 \rangle = \frac{1}{2} \int B^2(\vec{s}) [I(\vec{s}) \pm U(\vec{s}) \sin(\phi_{path} + \Delta\alpha)] d^2 \vec{s} \quad (6)$$

$$= \frac{1}{2} \left[\int B^2(\vec{s}) I(\vec{s}) d^2 \vec{s} \pm |V^U| \sin(\phi_U + \Delta\alpha) \right] \quad (7)$$

where I and U are the Stokes parameters as defined in [8]. The visibility V^U is the Fourier transform of the Stokes parameter U on a field defined by the beam :

$$V^U = \int B(\vec{s})^2 U(\vec{s}) e^{-i2\pi \frac{\vec{b} \cdot \vec{s}}{\lambda}} d^2 \vec{s} = |V^U| e^{i\phi_U}. \quad (8)$$

This visibility can be extracted from the measured signal by varying the phase shifts [9]. Using an OMT for each horn and a beam combiner with eight ports (four inputs and four outputs), equation (7) can be generalized and the visibilities of each 4 Stokes parameters are measured. All the polarized information on the sky is therefore recovered and hence the B-modes provided that the instrument has enough sensitivity and systematic cleanness [4, 10].

2 System analysis

An important issue to understand bolometric interferometry is systematic effects extraction and laboratory characterization. In order to be able to do that, we propose a method that allows to recover the system parameters by a set of both power and vectorial measurements.

A crucial point is to link in a coherent way the wide bandwidth power measurements and the monochromatic vectorial measurements. Using a VNA, we measure the S parameters, while with the power meter (or bolometer) we measure directly the power derived as a function of the incoming EM field. The integration of the VNA measurements in a bandwidth $\Delta\nu$ makes it necessary to

correctly simulate the behavior of the whole system (calibration of the integration window). For that purpose we consider the properties in term of S parameters for each component of the system and we deduce the theoretical power at the output. Then we show how to convert the properties encoded in the S-parameters into a more general formalism that allows to take into account the polarization states of the outgoing EM field.

2.1 Analysis method

There are two kinds of analysis we can use : two ports and four ports analysis. Each component of the instrument, apart the hybrid coupler, can be studied independently as a two ports device. With a VNA, we measure the corresponding [S] matrix which can be related to the [ABCD] matrix. The *ABCD* formalism is a very useful tool for the quasi-optical instrument analysis since it allows the propagation of the signal parameters linearly over the chain [11]. We use this analysis for all the two ports components along each channel of the instrument since there is no mixing between the incoming signals. However, this formalism does not take into account the two polarization states of the incoming EM field and their combination.

From the definition of the S parameters, we can deduce a relation between the incoming field $E_{k,1}$ and the outgoing field $E_{k,2}$ from a studied device k (see Appendix):

$$E_{k,2} = \left(\frac{S_{21}e^{-i\beta_2} + \left(\frac{S_{11}}{S_{12}}\right)e^{i\beta_2}}{e^{-i\beta_1} + S_{11}e^{i\beta_1}} \right) E_{k,1} \quad (9)$$

where $k \in (x, y)$.

This equation shows the relation satisfied by a single element of a Jones like matrix [8]:

$$\begin{bmatrix} E_{x2} \\ E_{y2} \end{bmatrix} = [J] \times \begin{bmatrix} E_{x1} \\ E_{y1} \end{bmatrix} \quad (10)$$

where E_{x1} and E_{x2} are respectively the input and the output fields in the x direction, E_{y1} and E_{y2} in the y direction and J a 2×2 matrix which can be written as:

$$[J] = \begin{bmatrix} J_x & \xi_x \\ \xi_y & J_y \end{bmatrix} \quad (11)$$

In equation (11), ξ_x and ξ_y allow the superposition of the two polarization states.

For a general four ports device or system, we will have $\xi_{x,y} \neq 0$. In order to extract the parameters of such a system, let's consider a device with the incoming ports (1,2) and the outgoing ports (3,4). In this case, $\xi_{x,y}$ expresses the transmission from port (1,2) to port (4,3) when $J_{x,y}$ represents the transmission from port (1,2) to port (3,4). With two matched loads at port (2) and (3), we can find ξ_x and using two matched loads at ports (1) and (4), we can find ξ_y . With the matched loads at the ports (2) and (4) we can recover J_x and at the ports (1) and (3) we can recover J_y . This allows us to reconstruct the signal in order to eliminate the systematic effects.

For our instrument, this can be used for both the hybrid coupler and the whole chain. In the output of the hybrid coupler, the power is expressed by equation (5).

3 Experimental setups

Looking at equation (7), it is clear that there are two kinds of measurements that can be done in order to demonstrate the basic operation of bolometric interferometry. The first one consists in varying ϕ_{path} with $\Delta\alpha$ fixed, while the other one is varying $\Delta\alpha$ with ϕ_{path} fixed. $\Delta\alpha$ is varied by changing the phase introduced by the phase shifters and ϕ_{path} is changed by rotating the source with respect to the phase center of the interferometer. The bolometric measurements have been done varying ϕ_{path} and $\Delta\alpha$ while the room temperature measurements fixed ϕ_{path} changing $\Delta\alpha$. In the following, the two setups are described.

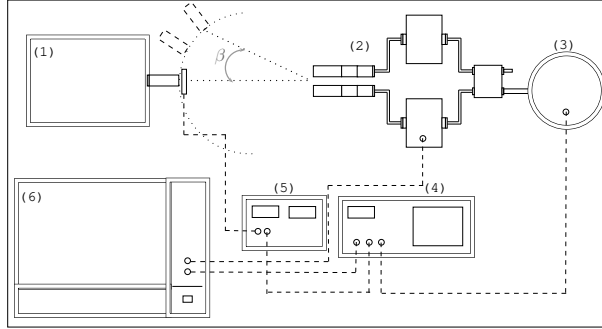


Figure 2: Experimental setup for bolometric measurements. (1) ABmm Vector Network Analyzer with the source polarized vertically, (2) The DIBO instrument, (3) Cryostat with the 4K bolometer, (4) Lock-in Amplifier, (5) Chopper, (6) Computer.

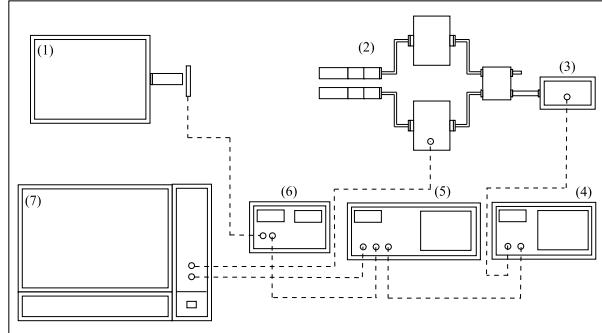


Figure 3: The set-up used for the characterization of the interferometer's response to broadband signals. (1) Farran BWO-10 power generator. (2) Demonstrator to be characterized. (3) HP W8486A power sensor. (4) HP 438A power meter. (5) EG&G 5209 lockin amplifier. (6) Chopper controller. (7) Computer for controllable phase variation and data acquisition.

3.1 Bolometric setup (4K)

We used an ABmm MVNA² as a monochromatic source and a 4 K cooled semiconductor bolometer³ read by a lock-in amplifier as a detector (figure 2).

In order to change ϕ_{path} , we move the instrument with respect to the source by an angle β as shown in figure 2. The distance between the two horns of the instrument is set to 20.5 cm and the gaussian beam of the emitting horn has a 1σ width of $\sim 4.2^\circ$ at 90 GHz.

3.2 Room temperature setup

In this section the experimental set-up used for power measurements around the nominal central frequency of DIBO (90 GHz) is described (figure 3). A frequency sweeper FARRAN BWO-10 is used as a source, operating both in Continuous Wave (CW) mode and in sweep mode. In the first case, a quasi-monochromatic signal is produced at a fixed frequency. In the second case, a frequency sweep across a chosen bandwidth (87-93 GHz, or 75-110 GHz in our case) is performed in 10 ms. The signals, collected by the two antennas of the interferometer, after phase shifting are combined in the hybrid, and then detected with a power sensor HP W8486A, placed on one of the two outputs of the combiner (the second one is closed on a matched load). Then, the analog output of the power meter HP 438A feeds a single channel lock-in amplifier EG&G 5209. The external reference of the lock-in is the driving signal coming from the control unit of the chopper, which modulates the source signal at 10 Hz. The basic idea behind this set-up is to replace an artificial black body with a fast frequency sweep across all the frequency band. If the sweep is much faster than the response time of the power meter (as in our case, since the typical time constant of the power sensor is $\tau = 35$ ms), this system can mimic a broad-band source. Of course the best solution would be an artificial black-body, but commercial power meters operating at room temperature are not sensitive enough to detect a 300- 500 K signal. This set-up can be useful for the characterization of millimeter-waves systems whenever cryogenic front-ends are not available.

We underline that even if the signal of the sweeper is strong enough to be directly detected by the power sensor, we preferred to use a lock-in in order to operate always with a favorable signal-to-noise ratio, even when the source's oscillator was used at power levels below the 25% of the peak power available. In fact below this threshold the sweeper's output power *vs* frequency is practically flat. For our purposes, using the instrument's specifications, we can estimate that $P_{83-97}/P_{75-110} \cong \Delta\nu_{83-97}/\Delta\nu_{75-110} = 0.17$: that is, the power delivered in a frequency range is essentially proportional to the bandwidth itself.

4 Results

4.1 Characterization

The S-matrix of every single microwave component has been obtained before assembling the full instrument. Then, the full interferometric chain, from the twist to the output ports of the hybrid, has been characterized in the same way, allowing us to get the transmission function of the full instrument. In such a system, the devices deserving the most careful characterization are phase shifters. In fact, commercial phase shifters behaves usually in a nearly ideal way when they are

²<http://www.abmillimetre.com/>

³IR lab

operated close to the center of the nominal frequency range, while some unwanted effects start to appear at other frequencies. In particular, we noticed that, going far from 90 GHz, (1) losses become increasingly important and (2) changing the phase settings produces an amplitude modulation of the incoming signal (see figure 4). Of course the point here is only to know and correctly recognize such effects, and eventually see how they propagate till the output of the system. At 90 GHz, the nominal center frequency, the power transmission coefficient is almost flat while the nominal phase setting of the device varies between 0 and 360 degrees: the values of $|S_{21}|$ in linear scale oscillates between 0.81 and 0.82. At 110 GHz, the same quantity is modulated between 0.36 and 0.84, while at 80 GHz between 0.77 and 0.87 (the same overall behavior and the same values are found measuring $|S_{12}|$, the device being reciprocal).

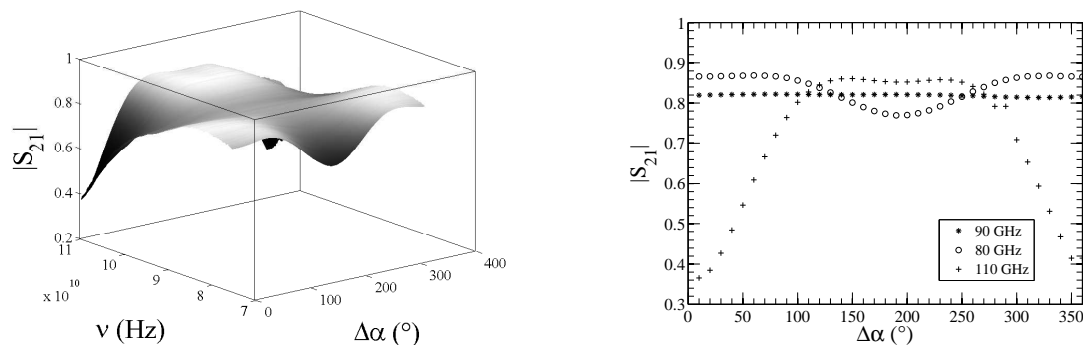


Figure 4: Right : $|S_{21}|$, for one phase shifter, as a function of $\Delta\alpha$ at 80, 90 and 110 GHz. Left : $|S_{21}|$ as a function of ν and $\Delta\alpha$.

We measured the behavior of the full chain at each frequency as a function of the phase introduced by the phase shifter with a VNA. We report here the received power as a function of the introduced phase shift. This power is normalized with respect to the ideal behavior of the instrument and represents the monochromatic transmission function. As we can see in figure 5, the instrument is designed to work at 90 GHz and its efficiency decreases when we switch to another frequency in the bandwidth 75-110 GHz. This is due to the fact that the devices are designed to work only close to the center frequency band. Moreover, we can observe that the amplitude does not depend only on the frequency but also on the phase. This effect is mainly due to the phase shifter.

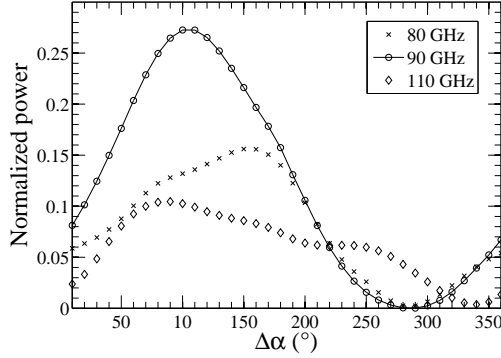


Figure 5: Normalized output power as a function of the phase shift (phase shifters) for three frequencies 80, 90, 110 GHz.

4.2 Bolometric measurements

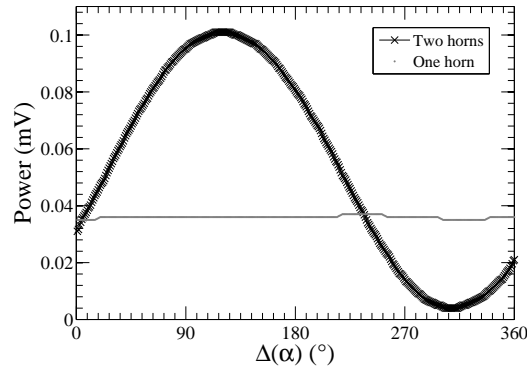


Figure 6: Measured signal from the bolometer with two horns (solid line) and hiding one of the horns (dot line).

Figure 6 shows bolometric measurements at 90 GHz by varying the phase shift $\Delta\alpha$ introduced by the phase shifters, β being fixed. As expected from equation (7), we observe a sinusoidal signal on the bolometer. Hiding one of the two horns, the observed interference disappears. The observed amplitude modulation is therefore produced by the interference and not by an amplitude modulation due to the phase shifters.

As shown on figure 2, we rotate the source with respect to the instrument by an angle β . We can therefore calculate from equation (7) the power at the output of the hybrid coupler as a function of the parameters of the setup:

$$P(\beta) = UB^2 \{1 + \sin[2\pi f \sin(\beta - \beta_0) + \theta]\} \quad (12)$$

where $f = \frac{D}{\lambda}$, D being the distance between the horns and β_0 an offset angle. θ is a factor that includes the phase shift $\Delta\alpha$ introduced by the phase shifters and other frequency dependent effects.

These effects can be due to the misalignment of the horns, the length difference of the channels and the non ideal behavior of the hybrid coupler and the phase shifters (Figure 4). U is the Stokes parameter of the source assumed to be a point source. In the case of a gaussian profile of the beam, we have: $B^2(\beta) = \exp\left(\frac{-(\beta-\beta_0)^2}{2\sigma^2}\right)$.

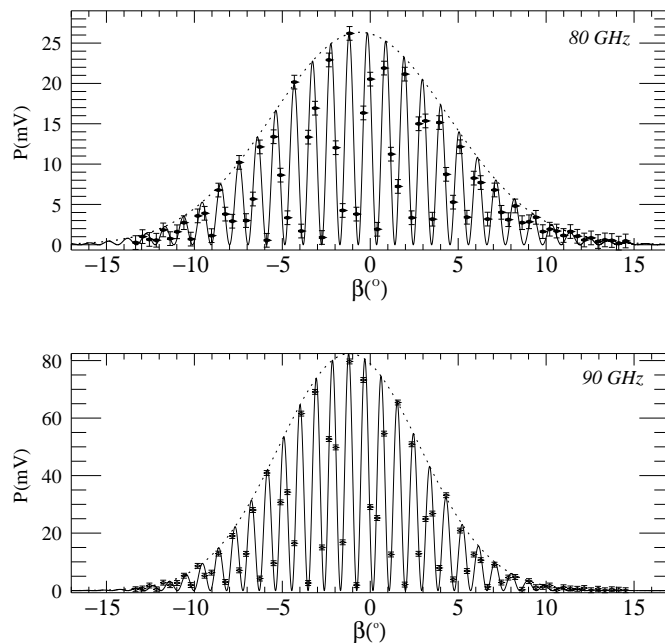


Figure 7: Measured signal (diamonds) and fitted fringes (solid line) as a function of the rotation angle with respect to the source at two frequencies (90 GHz and 80 GHz). The dashed line represents the gaussian envelope.

In figure 7 , we represent the measured power as a function of β at 80 GHz and 90 GHz. We also represent the fit of the equation (12) in the same figure. The values of the fitted parameters are showed in the table 1. The expected fringe frequency f is 54.7 ± 0.5 for $80GHz$ and 61.5 ± 0.6 for $90GHz$. We can see from table 1 that the expected values of f and σ ($\sim 4.2^\circ$ at 90 GHz) are close to the parameters extracted from the fit. The figure 7, therefore, shows the interference patterns from the two horns shaped by the beam.

ν	80 GHz	90GHz
U (mV)	13.17 ± 0.179	41.225 ± 0.199
β_0 ($^\circ$)	-0.58 ± 0.078	-1.18 ± 0.022
σ ($^\circ$)	5.01 ± 0.079	4.019 ± 0.022
f	54.97 ± 0.049	62.101 ± 0.021
θ ($^\circ$)	305.38 ± 27.065	106.75 ± 8.754

Table 1: Fit parameters of the equation 12 with $\chi^2 = 15.78$ for 90 GHz and $\chi^2 = 1.99$ for 80 GHz.

4.3 Room temperature measurements

As described in 3.2, the results showed here have been done with a system that mimics a broadband source. Figure 8 and ?? represent the power response of the system in arbitrary units. We can see then clearly interference patterns.

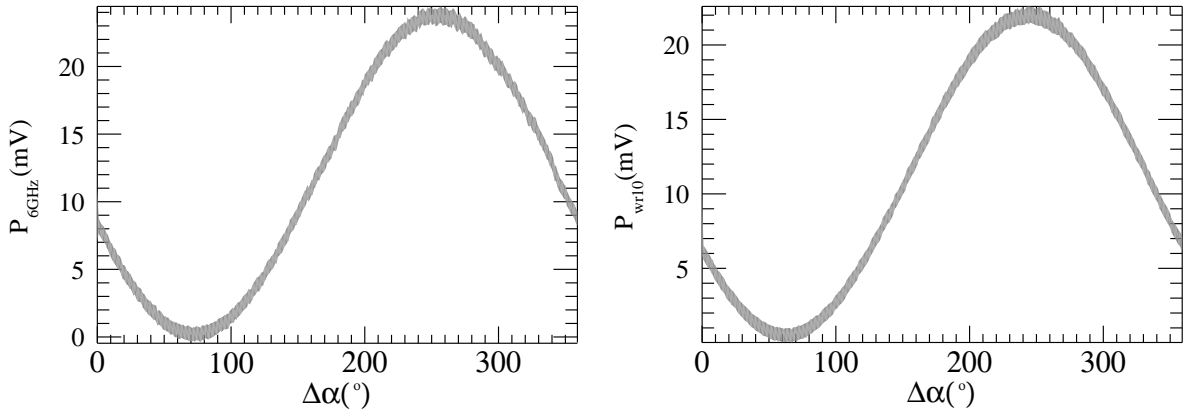


Figure 8: (a) Left: measured power with the room temperature bench in 6 GHz bandwidth around 90 GHz. (b) Right: measured power with the room temperature bench in the W band (between 75 GHz and 110 GHz).

4.3.1 Data analysis

Calibration factor

When performing measurements on a given bandwidth $\Delta\nu$, the system output is affected by the effect of bandwidth smearing. This effect alters the fringes frequency and compress their dynamic range, reducing their height. In order to verify the correctness of the power measurements and to try to disentangle the smearing effect from the systematics imprint, we have developed a strategy to compare power measurements with the monochromatic VNA ones. As a starting point, having the DIBO full chain transfer function and, starting from equation (5) and (10), we can reconstruct

the transmitted power as a function of the frequency and the phase shift

$$T_{power,i}^{VNA}(\nu, \Delta\phi) = (J_i + \xi_i)(J_i + \xi_i)^* \quad (13)$$

where $i = x, y$.

The link with the power measurements is made doing a very narrow band (CW) measurement at a frequency of 90 GHz to be compared with the transmitted power T_{power}^{VNA} ; comparing the correlated part of these measurements we have:

$$P(90GHz, \Delta\phi) = P_{inc}T_{power}^{VNA}(90GHz, \Delta\phi) \quad (14)$$

Through this relation we extract P_{inc} , the fractional power radiated by the sweeper and detected by DIBO. This parameter will be used as calibration factor for all the other power measurements. A transmitted power function can then be generated for finite bandwidth by:

$$T_{power}(\Delta\nu, \Delta\phi) = \frac{P(\Delta\nu, \Delta\phi)}{P_{inc}} \quad (15)$$

Numerically integrating T_{power}^{VNA} in the proper bandwidth range, we derive the expected power output starting from VNA data:

$$T_{power}^{VNA}(\Delta\nu, \Delta\phi) = \int_{\Delta\nu} T_{power}^{VNA}(\nu, \Delta\phi) d\nu \quad (16)$$

$T_{power}(\Delta\nu, \Delta\phi)$ and $T_{power}^{VNA}(\Delta\nu, \Delta\phi)$ are normalized with respect to the perfect behavior of the instrument before being compared.

Normalization

Recalling equation (10), the signal detected in the power meter sensor is the frequency integration of the square modulus of the linear combination of the incoming fields in the output of the hybrid. In an ideal case the transmission function has a rectangular shape so that the sinusoidal monochromatic response of the system is multiplied by a *sinc* function that depends on the bandwidth to give the integrated response

$$P = P_0 \left[1 \pm \sin\left(\frac{\pi\delta}{c}(\nu_1 + \nu_2)\right) \frac{\sin\left(\frac{\pi\delta}{c}\Delta\nu\right)}{\frac{\pi\delta}{c}\Delta\nu} \right] \quad (17)$$

where δ is the optical path difference, ν_1 and ν_2 the frequency boundaries, c the speed of light and $\Delta\nu$ the frequency bandwidth.

In the real case, we include the effect of the real transmission function calculated with the full chain VNA measurements. This transmission function is integrated in frequency with a numerical routine, to find the expected integrated behavior. In order to correctly normalize the results, we integrated also the ideal case response and normalized it to the expected value. This normalization factor is then applied to the real case integrated signal. Figures 9 and 10 show the comparison between the expected and the measured signal for both a 6 GHz band centered at 90 GHz and the full WR10 band respectively.

Complex degree of coherence

As we can see in table 2, there is a discrepancy between the expected and the measured data. To check if it is something due to the applied normalization we used, we calculate the modulus of the complex degree of coherence for both the simulated and the measured signals, according to its definition [12]:

$$|\gamma| = \frac{I_{max} - I_{min}}{I_{max} + I_{min}} \quad (18)$$

It turns out that the degrees of coherence for the simulated signals is comparable with those of the measured ones (at least within the error-bars), suggesting that the discrepancy is due to the normalization we introduce.

$ \gamma $	Measured	Simulated
6 GHz Band	0.96±0.04	0.94
WR10 Band	0.99±0.04	0.98

Table 2: Modulus of the complex degree of coherence computed for both the measured and simulated band integrated responses.

Systematic effects

A direct extraction of most of the systematics from the power signal cannot be performed since the error bars are greater than any of the imprint expected from them.

Anyway, some of the effects unveiled by the VNA characterization such as the amplitude distortion induced by the phase shifter are not seen because of the combined effect of the frequency integration of the signal and the low transmission of the instrument. That is, amplitude distortion is observed far from the central bandwidth frequency, where the transmission is very low (< -15 dB) so that their relative contribution to the output in the integration is negligible. This is confirmed by the fact that, in the numerical integration of the VNA (monochromatic) data, we do not observe these distortions. At some extent the frequency integration of the signal washes out systematics and this is particularly true for those affecting the signal far from the central frequency. This effect, acting also as a transmission reduction, mimics the shrinking of the effective bandwidth.

Finally, the normalization technique we used to compare simulated and measured data is based on the assumption that the calibration factor is the same at each frequency. If this is not true the frequency dependance of the calibration can introduce a different weighting in the integration, inducing distortions.

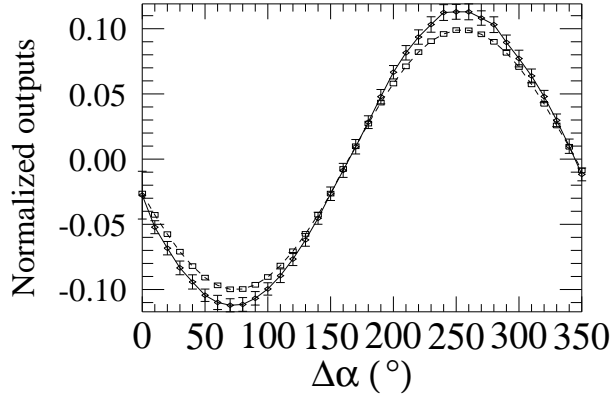


Figure 9: Comparison between the normalized correlated part of DIBO output signal (solid line) and the simulated one obtained integrating the VNA measurements (dashed line) for a 6 GHz band wide stimulus centered at 90 GHz.

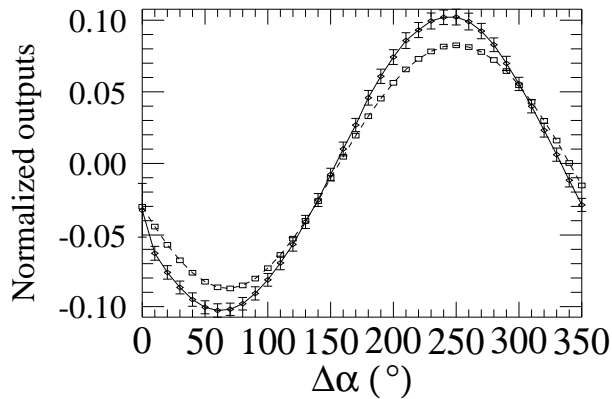


Figure 10: Comparison between the normalized correlated part of DIBO output signal (solid line) and the simulated one obtained integrating the VNA measurements (dashed line) for the full WR10 band wide stimulus.

5 Conclusion and future perspectives

With this demonstrator and a 4 K bolometer, the principle of bolometric interferometry has been proved with success in a laboratory environment.

This is the first attempt to understand how signals (their polarization properties) are altered propagating along the interferometer branches and how they interfere over a broad frequency band. In such a way we can study both the propagation of instrumental systematics and the effect of bandwidth smearing. To do so, we developed an experimental set-up that we used to illuminate the

interferometer over the WR10 frequency band, exploiting a fast sweeper able to cover the 75-110 GHz band in a fraction of the time constant of the commercial power meter used as detector. In this way, we have been able to check the very basic properties of the response of the full instrument at 300 K. In the second place, we have suggested a way of connecting the output of VNA measurements, the scattering parameters, first to the Jones matrices, and then to the modulated output power of the interferometer. The last one is an important point since it provides a link between the immediate output of microwave network analyzers, the S-matrix, and the elements of the Jones matrices often used by cosmologists to propagate instrumental systematics into astrophysical observables.

Even more important, illuminating the interferometer with an artificial source and detecting the signal with a 4 K bolometer, interference fringes have been clearly measured at two different frequencies (80 and 90 GHz). In this way, we could recover the expected fringe frequency.

In principle, a DIBO like architecture can be extended to a larger number of baselines and used in combination with other technologies. Indeed, to build a real bolometric interferometer (BRAIN/MBI), planar superconductor components (filters, phase shifters and detectors) will be considered as well as a beam combiner for the full power combination. It's worth underlining that DIBO is not an instrument designed to detect astronomical sources, but rather strong laboratory signals.

A future step will be the design of a more efficient demonstrator, endowed with more sensitive detectors, able to observe both polarized and unpolarized sources (artificial black-bodies). Then, having a more sensitive demonstrator, we can also test the capabilities of our conceptual scheme in unveiling systematics hidden in the modulated output of the interferometer. In fact, till now, we have just been able to recover the correct shape of the interference pattern calculated starting from the S-parameters of the full system. We remind that, in the present analysis, the behavior of the optical part of the experimental set-up has been considered Power6v1ideal. In the future, also an ad-hoc optical bench for the far field illumination of the next generation of demonstrators has to be designed, and a proper calibration strategy has to be foreseen.

Acknowledgements

This work has been done in the frame of the BRAIN/MBI collaboration, the CNES⁴/CNRS⁵ PhD funding for A. Ghribi and Ville de Paris Post-doc funding for A. Tartari. Special thanks to Alessandro Baù and Andrea Passerini for helping us in solving technical problems.

References

- [1] U. Seljak and M. Zaldarriaga, "Signature of gravity waves in the polarization of the microwave background," *Phys. Rev. Lett.*, vol. 78, no. 11, pp. 2054–2057, Mar 1997.
- [2] J. Puget, "Planck mission," *35th COSPAR Scientific Assembly*, 2004.
- [3] J. Bock *et al.*, "Task Force on Cosmic Microwave Background Research," 2006.
- [4] J.-C. Hamilton, R. Charlassier, C. Cressiot, J. Kaplan, M. Piat, and C. Rosset, "Sensitivity of a bolometric interferometer to the cosmic microwave background power spectrum," *A&A*, 2008.

⁴Centre des Etudes Spatiales du rayonnement

⁵Centre National de la Recherche Scientifique

- [5] M. White, J. E. Carlstrom, M. Dragovan, and W. L. Holzapfel, "Interferometric Observation of Cosmic Microwave Background Anisotropies," *The Astrophysical Journal*, vol. 514, pp. 12–24, Mar. 1999.
- [6] R. Charlassier for the BRAIN Collaboration, "The brain experiment, a bolometric interferometer dedicated to the cmb b-mode measurement," *Proceeding of the 43rd "Rencontres de Moriond" on Cosmology*, 2008.
- [7] S. Galli, "Bolometric interferometry demonstrator to measure the cosmic microwave background polarization," *AstroParticle & Cosmology*, Internship report, 2007.
- [8] M. J. Thompson, A.R. and J. G. Swenson, *Interferometry and Synthesis in Radio Astronomy*, Wiley-Interscience, Ed. Wiley-Interscience, 2001.
- [9] R. Charlassier, J.-C. Hamilton, É. Bréelle, A. Ghribi, Y. Giraud-Héraud, J. Kaplan, M. Piat, and D. Prêle, "An efficient phase-shifting scheme for bolometric additive interferometry," *ArXiv e-prints*, Jun. 2008.
- [10] E. Bunn, "Systematic errors in cosmic microwave background interferometry," *Physical Review D*, 2007.
- [11] D. M. Pozar, *Microwave Engineering*, J. W. . Sons, Ed. John Wiley & Sons, 1998.
- [12] A. B. B. Max Born, Emil Wolf, *Principles Optics*, C. U. Press, Ed. Cambridge University Press, 1999.

Appendix

A.1 Relation between the field and the S parameters

We consider here a two ports device. The source generator is connected to port 1 and a matched load to port 2. We then have an incident wave V_1^+ to the DUT (Device Under Test). The wave reflected from the device back to port 1 is V_1^- . The signal traveling through the DUT and toward port 2 is V_2^- . Any reflection from the load is V_2^+ . We can define S-parameters in terms of these voltage waves [11]:

$$\begin{aligned} S_{11} &= \frac{V_1^-}{V_1^+} & S_{12} &= \frac{V_1^-}{V_2^+} \\ S_{21} &= \frac{V_2^-}{V_1^+} & S_{22} &= \frac{V_2^-}{V_2^+} \end{aligned}$$

where S_{11} represents the input terminal reflection coefficient Γ_1 , S_{21} forward gain or loss, S_{12} Reverse gain or loss and S_{22} Output terminal reflection coefficient Γ_2 . We should underline that these parameters are normalized. Transient field, is, by opposition to the tangent field, the one propagating inside the waveguide. The tangent field is set to zero by the boundary conditions of the Maxwell equation to avoid surface current in the analysis.

We can express the transient E field in term of voltages:

$$\begin{aligned} E_1 &= \frac{e(x, y)}{c} (V_1^+ e^{-i\beta_1} + V_1^- e^{i\beta_1}) \\ E_2 &= \frac{e(x, y)}{c} (V_2^+ e^{-i\beta_2} + V_2^- e^{i\beta_2}) \end{aligned}$$

where $e(x, y)$ is the variation of the amplitude of the field propagating inside a waveguide section and c is a geometrical parameter. These variables are set to constants because of the common waveguide shape along the chain (cascade of components). E_1 and E_2 are the fields in the input and in the output of the device and β_1 and β_2 are their respective phases. In order to express E_2 with E_1 , we need to consider the same base (the same propagation direction of the wave). Let's set the propagation from port 1 to 2 as positive and from 2 to 1 as negative. This gives

$$E_2 = \frac{e(x, y)}{c} (V_2^+ e^{i\beta_2'} + V_2^- e^{-i\beta_2'})$$

with $\beta_2' = -\beta_2$

Finally, expressing E_2 as a function of E_1 , we obtain

$$E_2 = \left(\frac{S_{21} e^{-i\beta_2} + \left(\frac{S_{11}}{S_{12}} \right) e^{i\beta_2}}{e^{-i\beta_1} + S_{11} e^{i\beta_1}} \right) \times E_1$$

This relation is useful to make the link between the VNA measured S parameters and the propagating field for a two ports device. Also, it can be used to translate a 4 ports or double polarization propagation from an S matrix formalism into a Jones matrix formalism.

A.2 Relation between the S parameters and the ABCD parameters

The ABCD formalism allows to propagate the signal over a chain of two ports devices. The relation between the S parameters and ABCD parameter is given in [11].